Influence of Sodium (Na^{+1}) Ion doping on the Structural and Dielectric Nature of Lanthanum Chromite ($LaCrO_3$)

Dharmendra Mewada[1], Rajesh Kumar Katare[2]
[1,2]*Department of Physics, SAGE University, Indore (M.P.), 452020, India*

Abstract **- Hereby, we report solid synthetic route to synthesize $La1\text{-}_xNa_xCrO_3$ (x = 0.0, 0.05, 0.1) perovskite materials. These chromites were investigated for structural and dielectric properties. To establish the crystal structure acquired by the samples under study, we carried out X-ray diffraction, a reliable technique in addition to the Raman and FTIR characterizations. The XRD data analysis confirms orthorhombic (Pbnm) structure for all the samples. The phase formation was verified from the characteristic Raman modes of vibration and fingerprint absorption bands of the FTIR spectra. The structural analysis were polished by Rietveld Refinement of the XRD data that confirmed the above mentioned phase and other related structural parameters. Strain and particle size analysis was carried out by exploiting Williamson-Hall method. The room temperature dielectric study reveals the samples exhibit good dielectric constant and lower loss values. Jonscher's law fitting for frequency dependent ac conductivity reveals value of n < 1 which suggests frequent hopping of carriers with translational motion. Furthermore, the conduction was thrown light through electric modulus and impedance studies.**

Index Terms **- Chromites; Structure; Rietveld refinement, Dielectric properties; Jonscher's law.**

INTRODUCTION

The perovskite lanthanum chromite ($LaCrO_3$), a rare-earth oxide material has attracted research community for last few decades by virtue of its wide and interesting features indispensable for technological applications. It is a typical perovskite material with the general formula of ABO_3. Since, perovskites materials exhibit ubiquitous physical properties. The main features that enhance their usability in the modern device applications include their high thermal expansion coefficient, mechanical strength, better electronic conductivity and high melting point (≈ 2400 ^oC). Furthermore, they inherit stability from both physical and chemical aspects as it has higher stability for oxidation and corrosion thereby they are used in solid oxide fuel cells, sensors, catalysis etc. [1-3].

$LaCrO_3$ (LCO) is an insulating and optically transparent material exhibiting higher optical absorption at ≈ 4.6 eV8 arising from O 2p −→ Cr 3d charge-transfer excitation. The substitution of Na^{1+} for La^{3+} in LCO can induce the p-type conductivity via doping of holes into the top of the valence band [4, 5]. As perovskite structures are chemically and thermally stable, thereby making doping of the LCO very easy. Their enhanced applications are offered via combination with other n-type perovskite thereby giving rise to the formation of potential candidate for p-n junctions. In perovskite solar cells, the now-a day materials for solar cell applications, doping of LCO may stood as potential material. For solid oxide fuel cells applications, doped LCO has attracted the materials researchers from both theoretical and experimental point of view due to their bright future in advanced applications [4-6].

Bulk LCO usually exhibit an orthorhombic perovskite structure (space group Pbnm) with 20 atoms in the unit cell. It has a G-type anti-ferromagnetic insulating ground state below its Neel temperature (275 K). In high-spin configuration, every Cr^{3+} ion has three occupied t^3_{2g} states hybridized with 2p states of oxygen atoms in the vicinity, while the three other t^0_{2g} states and all e^0_g states are empty. The lowest energy transition in LCO originates from the Mott-Hubbard type transition[7-9].

Literature reveals that Cr oxides possess good electrical, magnetic, and structural properties. $LaCrO_3$ is antiferromagnetic below 290 K. The features that makes $LaCrO_3$ an essential interconnect material fuel cells and heating elements is its lower room temperature electrical conductivity, high thermal conductivity at extended temperature ranges and its stability at higher temperatures. There are reports that

throw light on electrical and magnetic properties of alkaline-earth doped $LaCrO_3$ at La-site [6,10].

$LaCrO_3$ is an interesting compound with transition metal ions that have three electrons in the 3d shell, which leads to total spin S= 3/2. The antiferromagnetic structure is G type, whereby each Cr^{3+} ion is anti-ferromagnetically coupled to its neighbour [10,11].

It has been synthesized by various techniques such as the hydrothermal method [12], the sol–gel method [13], the glycine nitrate method [14], the hydrazine method [15], etc. In this study we report the effects on the structural and electrical properties via doping of Na^{+1} cation on $LaCrO_3$ synthesized by the solid state reaction method. The lower valent ions are reported to enhance the sinterability, magnetization, and conductivity of lanthanum chromite [16]. There is hardly any report that provides details about structural and electrical with the substitution of Na^{+1} cation in the matrix of $LaCrO_3$.

EXPERIMENTATION

Synthesis

$La_{1-x}Na_xCrO_3$ (x = 0.0, 0.05, 0.1) perovskite materials were synthesized by the high temperature solid state reaction route. The precursors used were La_2O_3, Cr_2O_3, and Na_2CO_3. The precursors were weighed in appropriate proportions fixed via proper calculations upto 3decimal places. We mixed these precursors via mechanical grinding using an agate –mortar for 5h with intermediate addition of acetone to make proper dispersity of the ions throughout the sample. The powdered material was calcined for 800 ^oC for 6h. The calcined mixture was once again ground for 5h and re-calcined for the same time duration. The double calcined powder was finally ground for 1h to get fine powder ready for different characterizations. Some amount of this powdered was transformed into circular pellets with 1mm diameter and 1.2m in thickness. The pellets were sintered at 1000oC for 5h. The compact sintered pellets were polished by silver paste for electrical measurements.

$La_{1-x}Na_xCrO_3$ (x = 0.0, 0.05, 0.1) samples were X-ray diffraction (XRD) characterized to confirm the phase and crystal structure acquired by the $La_{1-x}Na_xCrO_3$ (x = 0.0, 0.05, 0.1) sample employing Bruker D8 advanced X-ray diffractometer with CuKα1 radiation (λ=1.54060Å), in the angular range from $20^o < 2\theta < 80^o$. Employing LABRAM - HR800 spectrometer equipped with a 50 × objective and a Peltier-cooled charge coupled device detector, we recorded Raman spectra excited with 488 nm radiations (2.53 eV) from an air-cooled Argon Laser. The instrument used for dielectric measurements on $La_{1-x}Na_xCrO_3$ (x = 0.0, 0.05, 0.1), the lanthanum chromites was Model E4980A Precision LCR meter (2Hz-2MHz) from Keysight Technologies.

RESULTS AND DISCUSSIONS

XRD Analysis

The bulk and polycrystalline $La_{1-x}Na_xCrO_3$ (x = 0.0, 0.05, 0.1) lanthanum chromites synthesized via solid state reaction route were examined for phase formation and crystal structure using XRD technique and the data was recorded in the angular range of 10^o to 80^o. The data was plotted and displayed as Figure 1. From the analysis of the XRD patterns, it was found that all the samples are identical evident from the similar XRD patterns. Furthermore, these samples were found to have crystallized in orthorhombic structure (Pbnm) [17]. The absence of any deviation in the XRD pattern and appearance of any new peak infer that the acquired crystal structure is same attributed to the proper dispersion of Na-ions at La site. The decrease in the intensity of characteristic XRD peaks is attributed to the defects created via doping. The samples are highly crystalline and have higher average particle size evident from the sharpness and narrow FWHM of the characteristic XRD peaks. The average crystallite size was calculated by the classical Scherer formula and the obtained 115 nm, 99nm and 122nm respectively for $La_{1-x}Na_xCrO_3$ (x = 0.0, 0.05, 0.1) samples.

To further emphasize on the structure and establishment of results discussed in the XRD data analysis, we performed Rietveld Refinement using FullProf software of 10% doped LCO displayed as Figure 2. The various structure related parameters obtained from the refinement of the XRD data are demonstrated in the Table 1.

Furthermore, we explored the strain induced in the sample via Na doping and the average size of the crystallites using Willaimson-Halll technique [18]. The W-H plot for the 10% doped LCO is displayed as Figure 3. The linear data fitting provides the average crystallite size to be 160nm and strain of the order of 1.15*10^-3 displayed within the W-H plot displayed as Figure 3.

FTIR Analysis

Figure 4 presents the FTIR spectrum of $La_{1-x}Na_xCrO_3$ (x = 0.0, 0.05, 0.1) samples of lanthanum chromite. Recorded in the wavenumber range of 400 and 4000 cm^{-1}. The absorption band appearing at 405 cm^{-1} is an attribute of stretching of O–Cr–O bond whereas the band evident at 564 cm^{-1} is ascribed to Cr–O vibration mode stretching. The bands lying in the higher frequency range viz. 800–475 cm^{-1} centered around 540 cm^{-1} arise from stretching vibrations, whereas the absorption bands falling in the wavenumber ranging from the 475 cm^{-1} to 300 cm^{-1} in the region of low frequency centered around 400 cm^{-1} arise from bending of metal oxygen bonds [19-21]. The as observed absorption band confirms the desired phase formation.

Raman Analysis

Figure 5 shows Raman spectra of $La_{1-x}Na_xCrO_3$ (x = 0.0, 0.05, 0.1) samples of lanthanum chromite. The spectra presents a vibration mode at 585 cm^{-1} denoted as as B_{3g} (3) attributed to O_2 and O_1 anti-stretching, the mode of vibration appearing at 430 cm^{-1} denoted by A_g (6) arises from bending of BO_6, atomic motion along axes give birth to the mode appearing at 238 cm^{-1} is due to atomic motions, i.e., O_1 (x), A (-x) awaken via distortion, attribute of A shift and denoted as A_g (4), vibration mode at 155 cm^{-1} [Ag (2)] appears due to A(z) from out of plane motion [22-24]. The modes of vibration that appear in the wavenumber range higher than 600 cm^{-1} are unusually normal modes for $La_{1-x}Na_xCrO_3$ (x = 0.0, 0.05, 0.1) samples of lanthanum chromite. However for the Raman spectra of $La_{1-x}Na_xCrO_3$ (x = 0.0, 0.05, 0.1) samples, the vibration in the range of 600–200 cm^{-1} are witnessed from the available literature. Therefore, higher oxidation state of chromium are expected to give arise to the vibration at higher wavenumber values [22-26].

Dielectric Studies

The complex form of dielectric function in an applied field can be expressed in terms of an equation $\varepsilon = \varepsilon' + i\varepsilon''$, where the real part, i.e., ε' is the relative dielectric constant and represents the polarization oriented energy storage capacity and is mostly frequency and applied external field dependent. The imaginary part, i.e., ε'' represents the energy dissipation term, and its value was calculated by the relation: $\varepsilon'' = \varepsilon' \times \tan\delta$. The ratio tand = $\varepsilon''/\varepsilon'$ represents the dissipation factor, and δ is the phase difference between the induced current and applied field.

The room temperature frequency dependent dielectric constant of $La_{1-x}Na_xCrO_3$ (x = 0.0, 0.05, 0.1) samples in the frequency range of 100 kHz – 2 MHz is displayed as Figure 6. It is evident from the graph that with increase in frequency, the dielectric constant (ε') decreases. The decrease in dielectric constant is sharp in the region of low frequency and becomes very less responsive to the applied field in the higher frequency side. This behaviour is common for ceramic materials when dipoles induced in the dielectric medium do not follow the applied field frequency thereby leads to the reduced dielectric constant value in the higher region of field. The value of dielectric constant, ε' is high for the lower values of applied field which is attributed to the interfacial polarization arising from the piling up of surface charges at the grains boundaries explained in terms of Maxwell-Wagner model [27]. According to M-W model, the grains conducting in nature are shielded by non-conducting grain boundaries and charges move easily with applied field and pile up at the grain boundaries in the low frequency regions as they align properly leading to higher polarization and hence the dielectric constant whereas they hardly get time to align in the higher frequency values where reversal motion happens thereby dielectric constant decreases. Furthermore, it is noticed that with the doping of Na^{+1} ions, the dielectric constant decreases which might occur due to structural inhomogeneties and lattice defects induced in the sample.

Figure 7 displays dielectric loss, tanδ for $La_{1-x}Na_xCrO_3$ (x = 0.0, 0.05, 0.1) lanthanum chromite samples. The dielectric loss is observed to decrease with rise in frequency values. The value of tanδ is higher at low frequency region and vice versa arising from surface charge effect. However, tanδ suffers reduction with rise in frequency and metal ions loss ability to follow the variations in the applied field, thereby resulting in decrease of dielectric loss values [28, 29]. In addition to this, frequency dependence of dielectric loss is highly impacted with the doping. The pristine LCO possesses higher loss values which decreases with increases in Na^{+1} concentration. The as synthesized $La_{1-x}Na_xCrO_3$ (x = 0.0, 0.05, 0.1) lanthanum chromite materials have the combination of relatively high dielectric constant and low losses which makes them suitable as dielectric materials for ceramic capacitors and other electronic devices

operating at high temperatures [30,31]. This observation further appeals to go for temperature dependent dielectric measurements to establish their position in the electronic device applications.

***ac* conductivity**

Figure 8 shows the variation of σ_{ac} of $La_{1-x}Na_xCrO_3$ (x = 0.0, 0.05, 0.1) lanthanum chromite materials as a function of frequency. The plateau region and the dispersion region are the two regions of the Figure 8 of conductivity within the bound of frequency [32-34]. Plateau region is low frequency region where as high frequency regions represents dispersion. In the low frequency region, conductivity does not follow frequency and comprises of *dc c*onductivity whereas dispersion region corresponds frequency dependent. Jonscher's law i.e $\sigma_{ac} = \sigma_{dc} + A\ \omega^n$, where n is a constant and dimensionless frequency exponent, A is dispersion parameter and it represents the polarizability strength and hence the interaction of mobile ions and lattices , is exploited to throw light on the *ac* conductivity depending on frequency. The relation $n > 1$ suggests localized hoping of the entity without leaving the local environment and the relation $n < 1$ suggests translational motion with abrupt hoping. Since our results show the relation $n < 1$ i.e. $0.2 < n < 0.3$, which therefore suggest frequent hopping of carriers with translational motion. The relaxation phenomenon that comes into existence via sudden hopping of charges provides the base to frequency dependent conductivity as stated by Jonscher's Law. The reason can also be the small value of band gap of the sample [29, 35].

ELECTRIC MODULUS STUDIES

Complex electric modulus analysis facilitates understanding the response that discriminates the nature of defects in the vicinity from electrode effect. It helps us to emphasize on the relaxation of applied field for constant dielectric polarization. Frequency dependent M′ as displayed in Figure 9 demonstrates irresponsive M′ in the low-frequency region and then increases with the rise in the applied field values presenting the dispersion in the material. The continuous increase in M′ is the result of short-range mobility of charge carriers that boost conduction process. It is related to the absence of restoring forces governing mobility of charge carriers under the influence of applied *ac* field. For low frequency regions, the low M′ indicates the presence of charge carriers with long-range mobility. Furthermore, it is worth to mention here that conduction phenomena has hardly any contribution from the electrode polarization [36].

Figure 10 presents the frequency dependence of M″ where M″ increases with increase in frequency. The frequency regime sensitive to the applied *ac* field describes the long-range movement of charge carrier. The low values of M″, in the low frequency region, indicate negligible contribution of the electrode polarization to the electric modulus [37].

To study the contribution of various microscopic elements, such as intra-grain and inter-grain electrode effect, and relaxation process, Cole–Cole plot analysis was used. Figure 11 shows the Cole–Cole plot of the compound corresponding to 20 Hz to 1 MHz. The resulting curve showed a tendency to bend towards the abscissa to form a semicircle with its centre below the real axis, having a comparatively larger radius and hence revealing an evident differentiation from the ideal Debye-type behaviour attributed to several factors such as grain orientation, grain boundary, stress–strain phenomena, and atomic defect distribution [36-37].

IMPEDANCE STUDIES

A widely followed concept in the appearance of two semicircles in the case of polycrystalline materials is that they stand for the relaxation processes in grain and grain boundaries, respectively. Figure 12 displays Nyquist plot of the as synthesized samples that exhibit the same characteristics. The figure displays two semicircles corresponding to high frequency region and middle frequency region. The semicircle present in the high frequency region arise from the charge transfer resistance at the electrolyte/electrode interface, whereas the semicircle lying in the middle region of frequency indicates charge transfer resistance in the photo-anode. From Nyquist plot, the small size of the semicircle in the middle of the frequency region for pristine LCO compared to 10% doped LCO indicates change in electron transfer process in photo-anode. Furthermore, the first semicircle in the Nyquist plot arises from the grains and the second one is the effect of grain boundaries.

The results are supported in the *ac* conductivity studies above [37, 38].

CONCLUSIONS

We successfully synthesized of $La_{1-x}Na_xCrO_3$ (x = 0.0, 0.05, 0.1) lanthanum chromite materials by the high temperature and convenient solid state reaction route. The synthesized samples were found to have crystallized into orthorhombic phase (Pbnm). The Rietveld refinement of the diffraction data confirms the467ormatione and related other parameters. Raman data analysis confirms lattice formation and FTIR supports the467ormationn of desired compound. The dielectric study conveys that all the as synthesized samples exhibits good dielectric character. The *ac* conductivity exploiting Jonscher's law reveals frequent hopping of carriers with translational motion. From impedance study, Nyquist plots show contribution to the conduction from grains and grain boundaries via display of two incomplete semicircles. Furthermore, non-Debye character with distribution of time relations is witnessed.

ACKNOWLEDGEMENTS

Authors gladly acknowledge the institute, UGC-DAE CSR, Indore (M.P.) India for characterization facilities. We express our gratitude towards Dr. D.M. Phase, center director, Dr. Mukul Gupta, Dr. V. G. Sathe, Dr. U. Deshpande, Dr. R. Rawat for guidance and discussions. Dr. Netram Kaurav, Holkar Science College is acknowledged for support.

REFERENCES

[1] E. Fortunato, D. Ginley, H. Hosono and D. C. Paine, MRS Bull. 32 (2007) 242.
[2] R. M. P. Barquinha, L. Pereira and E. Fortunato, Transparent Oxide Electronics: From Materials to Devices 1st edn (Chichester: Wiley).
[3] C. G. Granqvist, Sol. Energy Mater. Sol. Cells, 91 (2007) 1529.
[4] P. V. Sushko, L. Qiao, M. Bowden, T. Varga, G. J. Exarhos, F. K. Urban, D. Barton and S. A. Chambers, Phys. Rev. Lett., 110 (2013) 077401
[5] T. Arima and Y. Tokura, J. Phys. Soc. Jpn., , 64 (1995) 2488
[6] K. Tezuka, Y. Hinatsu, A. Nakamura, T. Inami, Y. Shimojo, and Y. Morii, J. Solid State Chem. 141, (1998) 404.
[7] T. Arima, Y. Tokura and J. B. Torrance, Phys. Rev. B, 48 (1993) 17006.
[8] K. Maiti and D. D. Sarma, Phys. Rev. B, 54 (1996) 7816
[9] W. C. Koehler and E. O. Wollan, J. Phys. Chem. Solids, 2 (1957) 100
[10] N. Sakai, H. Fjellvåg, and B. C. Hauback, J. Solid State Chem. 121 (1996) 202
[11] J. B. Goodenough, Phys. Rev. 100 (1955) 564.
[12] L. P. Vázquez, J. C. Rendón-Angeles, J. L. Rodríguez-Galicia, C. A. Gutiérrez-Chavarria, K. J. Zhu, K. Yanagisawa, J. Euro. Cera. Soci. 26 (2006) 81–88
[13] H. N. Girish, G. Q. Shao, B. Basavalingu, Roy. Soci. Chem. 6 (2016) 79763–79767
[14] Y. K. Lee and J. W. Park, Mat. Chem and Phys, 45 (1966) 97-102.
[15] M. R. De Guire, S. E. Dorris, R. B. Poeppel, S. Morissette and U. Balachandran, Journal of Materials Research, 8 (1993) 2327-2335
[16] Z. W. Zhong and Y. Mi, "Journal of Zhejiang University, 5 (2004) 1471
[17] L. Liu, M. Jiang, J. Yin, W. Guo, T.Jiao,Appl. Sci. 10 (2020) 4634.
[18] I. Jitaru, D. Berger, V. Fruth, A. Novac, N. Stanica and F. Rusu, Ceram. Int. 26, 193 (2000).
[19] V. S. Shinde, K. H. Kapadnis, C. P. Sawant, J. Emer. Techn. Inno. Res. (JETIR) 5(12) (2018) 546.
[20] W. Zheng, W. Pang, G. Meng and D. Peng, J. Mater. Chem. 9, 2833 (1999).
[21] M. Saleem, S. Tiwari, M. Soni, N. Bajpai and A. Mishra, International Journal of Modern Physics B 34 (2020) 2050033
[22] A. M. Glazer, Acta Crystallographica B 28 (1972) 3384.
[23] M. N. Iliev, M. V. Abrashev, H. G. Lee, V. N. Popov, Y. Y. Sun, C. Thomsen, R. L. Meng and C. W. Chu, Phys. Rev. B (Condensed Matter) 57 (1998) 2872.
[24] W. Rativa-Parada, J. A. Gómez-Cuaspud, E. Vera-López and J. B. Carda, IOP Conf. Series: Journal of Physics: Conf. Series 786 (2017) 012029

[25] D. L. Hoang, A. Dittmar, M. Schneider, A. Turnschke, H. Lieske, K.-W. Brzezinka and K. Witke, Thermochim. Acta 400 (2003) 153.
[26] M. N. Iliev, A. P. Litvinchuk, V. G. Hadjiev, Y.-Q. Wang, J. Cmaidalka, R.-L. Meng, Y.-Y. Sun, N. Kolev and M. V. Abrashev, Phys. Rev. B 74 (2006) 214301.
[27] Wagner K W 1913 Ann Phys. 40 817
[28] Koops C G 1951 Phys. Rev. 83 121
[29] S. M. Khetre, A. U. Chopade, C. J. Khilare, H. V. Jadhav, P. N. Jagadale, S. R. Bamane, J Mater Sci: Mater Electron, doi:10.1007/s10854-0131411-z
[30] K. K. Mallick, P. Shephered, R. J. Green, J. Eur Ceram Soc 27 (2007) 2045
[31] Y. Zhi, A. Chen, J. Appl Phys, 9 (2002) 794
[32] N. Bajpai, M. Saleem, S. Tiwari, M. Soni, and A. Mishra, AIP Conference Proceedings 2220, (2020) 040029.
[33] S. Tiwari, M. Saleem, N. Bajpai, M. Soni, and A. Mishra, AIP Conference Proceedings 2220 (2020) 040011
[34] M. Saleem and D. Varshney, RSC Adv. 8 (2018) 1600
[35] A.K. Jonscher. Universal Relaxation Law, ChelseaDielectricsPress, London, 1996
[36] A. Dh ahri,E. Dhahri, E. K. Hill, RSC Adv, 8 (2018) 9103
[37] S. Hcini, S. Zemni, A. Triki, H. Rahmouni, and M,. BoudardJ. Alloya Compd, 509 (2011) 1394
[38] B. A. yezer, A. S. Khair, P. J.Sides, D. C. Prieve, Journal of Colloid and Interface Science 469 (2016) 325

Figure Captions

Figure 1: Room temperature X-ray diffraction patterns of La1-xNaxCrO3 (x = 0.0, 0.05, 0.1) lanthanum chromite materials

Figure 2: Rietveld Refinement of 10% doped LaCrO3 lanthanum chromite sample.

Figure 3: Williamson-Hall plot of La0.9Na0.1CrO3 lanthanum chromite material.

Figure 4: Raman inelastic spectra of La1-xNaxCrO3 (x = 0.0, 0.05, 0.1) lanthanum chromite materials.

Figure 5: FTIR spectra of La1-xNaxCrO3 (x = 0.0, 0.05, 0.1) lanthanum chromite materials

Figure 6: Frequency dependent room temperature dielectric constant of La1-xNaxCrO3 (x = 0.0, 0.05, 0.1) lanthanum chromite materials

Figure 7: Room temperature frequency dependent dielectric loss of La1-xNaxCrO3 (x = 0.0, 0.05, 0.1) lanthanum chromite materials.

Figure 8: Frequency dependent room temperature Jonscher's law fitted ac conductivity of La1-xNaxCrO3 (x = 0.0, 0.05, 0.1) lanthanum chromite materials.

Figure 9: Room temperature frequency dependent Electric Modulus (M′) of La1-xNaxCrO3 (x = 0.0, 0.05, 0.1) lanthanum chromite materials

Figure 10: Electric Modulus (M″) of La1-xNaxCrO3 (x = 0.0, 0.05, 0.1) lanthanum chromite materials.

Figure 11: Cole-Cole plot for La1-xNaxCrO3 (x = 0.0, 0.05, 0.1) chromites.

Figure 12: Nyquist plot for La1-xNaxCrO3 (x = 0.0, 0.05, 0.1) lanthanum chromites

Table 1: Structural parameters obtained from Rietveld refinement of $La_{0.9}Na_{0.1}CrO_3$ chromite sample

Parameters	Obtained Values
Structure	Orthorhombic
Space group	Pbnm
a (Å)	5.499
b (Å)	5.49
c (Å)	7.76
V $(Å)^3$	234.13
Density (g/cm^3)	3.72
R_p	36.4
R_{wp}	12.5
R_{exp}	5.64
R_{Bragg}	20.3
Rf	14.4
GOF	2.2
χ^2	3.94

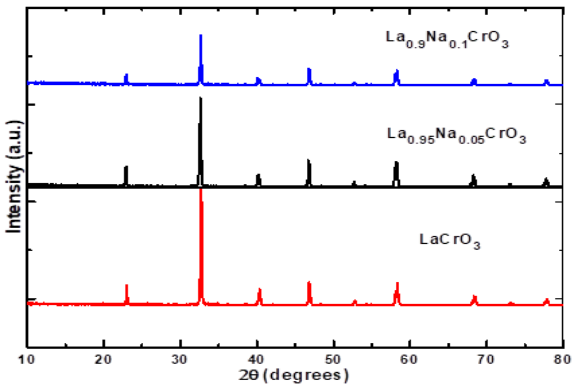

Figure 1

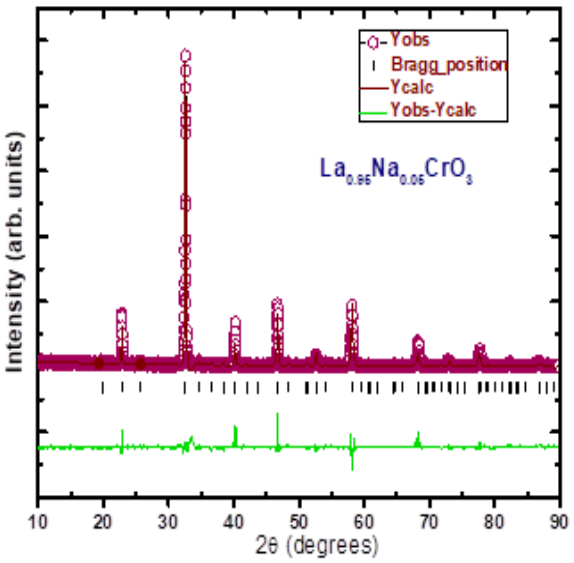

Figure 2

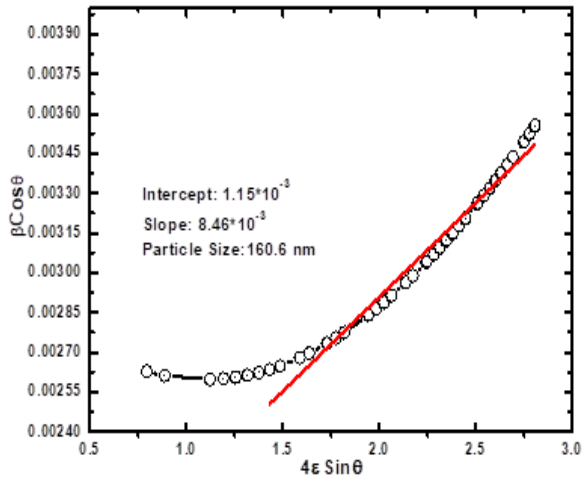

Figure3

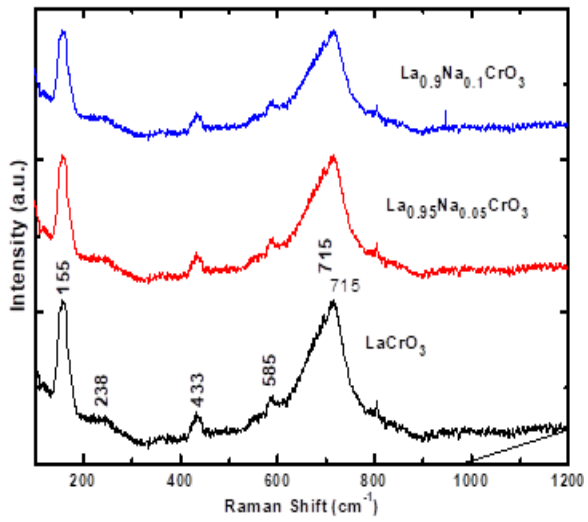

Figure 4

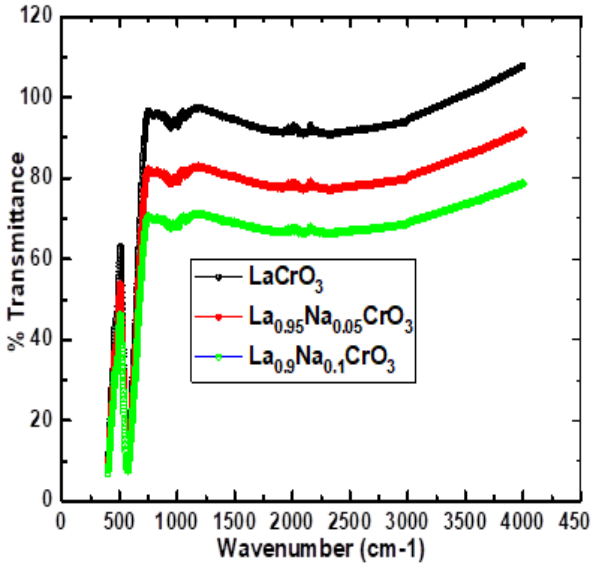

Figure 5

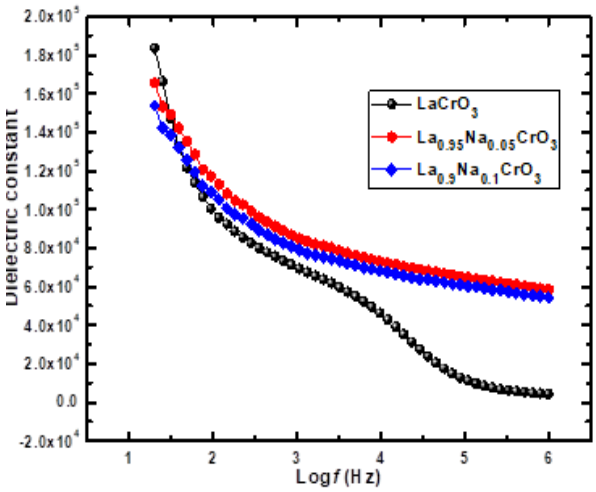

Figure 6

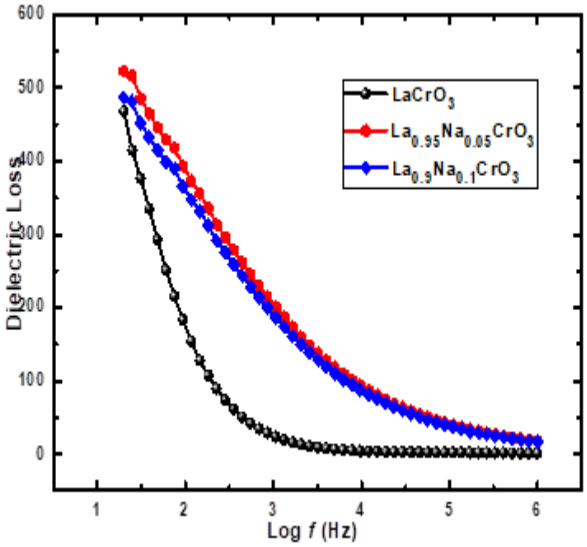

Figure 7

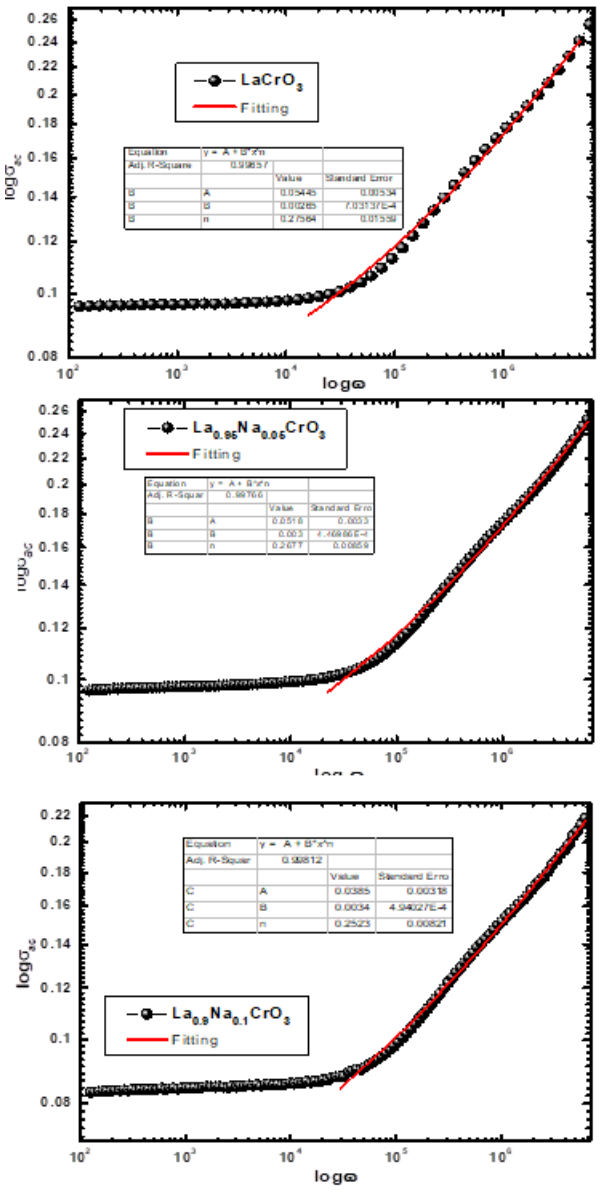

Figure 8

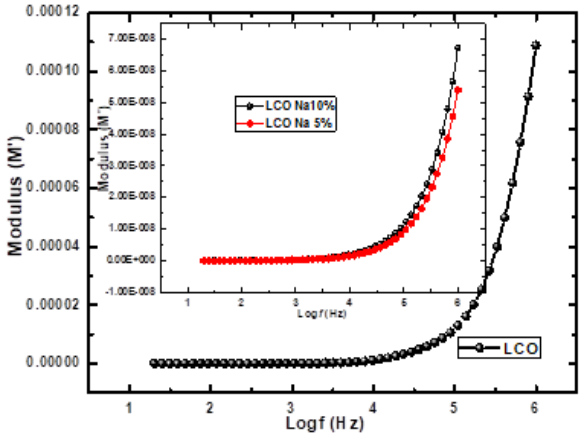

Figure 9

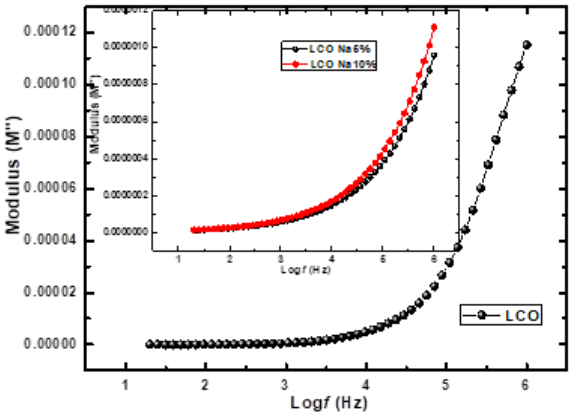

Figure 10

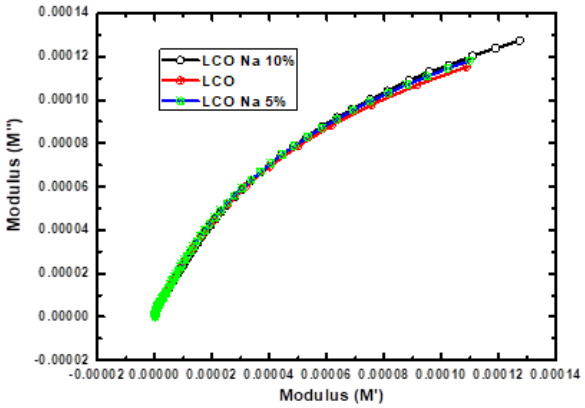

Figure 11

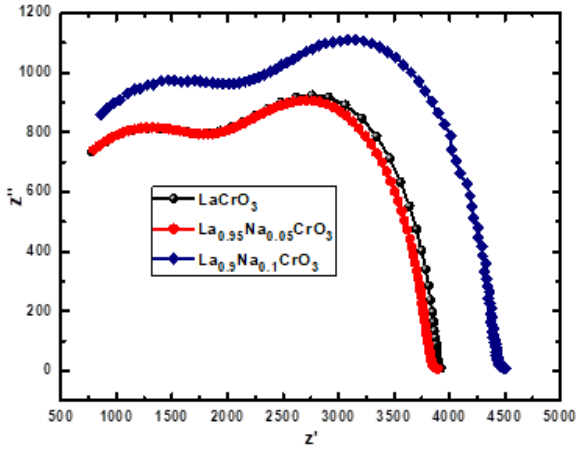

Figure 12